Published in final edited form as:
Cancer Res. 2008 October 15; 68(20): 8597–8606. doi:10.1158/0008-5472.CAN-08-0677.

Noninvasive Molecular Imaging of Hypoxia in Human Xenografts: Comparing Hypoxia-Induced Gene Expression with Endogenous and Exogenous Hypoxia Markers

Fuqiu He[1], **Xuelong Deng**[1], **Bixiu Wen**[1], **Yueping Liu**[1], **Xiaorong Sun**[2], **Ligang Xing**[1], **Akiko Minami**[1], **Yunhong Huang**[1], **Qing Chen**[2], **Pat B. Zanzonico**[2], **C. Clifton Ling**[2], and **Gloria C. Li**[1,2]

[1] Department of Radiation Oncology, Memorial Sloan-Kettering Cancer Center, New York, New York

[2] Department of Medical Physics, Memorial Sloan-Kettering Cancer Center, New York, New York

Abstract

Tumor hypoxia is important in the development and treatment of human cancers. We have developed a novel xenograft model for studying and imaging of hypoxia-induced gene expression. A hypoxia-inducible dual reporter herpes simplex virus type 1 thymidine kinase and enhanced green fluorescence protein (HSV1-TKeGFP), under the control of hypoxia response element (9HRE), was stably transfected into human colorectal HT29 cancer cells. Selected clones were further enriched by repeated live cell sorting gated for hypoxia-induced eGFP expression. Fluorescent microscopy, fluorescence-activated cell sorting, and radioactive substrate trapping assays showed strong hypoxia-induced expression of eGFP and HSV1-tk enzyme in the HT29-9HRE cells *in vitro*. Sequential micropositron emission tomography (PET) imaging of tumor-bearing animals, using the hypoxic cell tracer ^{18}F-FMISO and the reporter substrate ^{124}I-FIAU, yielded similar tumor hypoxia images for the HT29-9HRE xenograft but not in the parental HT29 tumor. Using autoradiography and IHC, detailed spatial distributions in tumor sections were obtained and compared for the following hypoxia-associated biomarkers in the HT29-9HRE xenograft: ^{124}I-FIAU, ^{18}F-FMISO, Hoechst (perfusion), lectin-TRITC (functional blood vessels), eGFP, pimonidazole, EF5, and CA9. Intratumoral distributions of ^{124}I-FIAU and ^{18}F-FMISO were similar, and eGFP, pimonidazole, EF5, and CA9 colocalized in the same areas but not in well-perfused regions that were positive for Hoechst and lectin-TRITC. In enabling the detection of hypoxia-induced molecular events and mapping their distribution *in vivo* with serial noninvasive positron emission tomography imaging, and multiple variable analysis with immunohistochemistry and fluorescence microscopy, this human xenograft model provides a valuable tool for studying tumor hypoxia and in validating existing and future exogenous markers for tumor hypoxia.

Introduction

Although the existence of tumor hypoxia has been suggested by Thomlinson and Gray (1) more than 50 years ago, its true importance in cancer management has only become known within the last 15 years. This is in part due to recent advances in methods to measure hypoxia,

Requests for reprints: Gloria C. Li, Memorial Sloan-Kettering Cancer Center, Box 72, 1275 York Avenue, New York, NY 10021. Phone: 646-888-2118; Fax: 646-422-0247; E-mail: lig@mskcc.org.

Disclosure of Potential Conflicts of Interest
No potential conflicts of interest were disclosed.

improved understanding of the molecular events associated with tumor hypoxia, and clinical findings correlating tumor hypoxia and treatment outcome (2–9). Importantly, numerous clinical studies, using physical probes to measure PO_2 levels, has shown that existence of tumor hypoxia is negatively correlated with local control and survival (2,3,10,11). Because hypoxic cells are 3-fold more radioresistant than aerated cells, such clinical results from radiotherapy trials are not surprising. However, Hockel and colleagues (10) reported similar findings for surgical patients who did not receive radiation treatment; the underlying reasons are now beginning to be understood.

It is now known that tumor hypoxia is associated with more aggressive tumor phenotypes (12–14), which may lead to poorer prognosis for patients with hypoxic tumors whether they are treated with surgery or radiation (5,15). Not only is the hypoxic environment selective for genetically unstable tumor cells, hypoxia is also associated with tumors that are more likely to metastasize (3,5,16–18). Such tumor phenotypes are due in part to the hypoxia-associated molecular pathways, which regulate the expression of many genes, including those involved in tumor progression and malignant phenotypes. At the molecular level, hypoxia-inducible factor 1 (HIF-1) has been identified as the “switch” (19,20). It is up-regulated in response to oxygen deprivation, binds to the hypoxia responsive element (HRE), and controls the transcriptional activity of numerous downstream genes that are important to the development and growth of solid tumors (21).

Its importance in cancer management has motivated much research in measuring, characterizing, and understanding tumor hypoxia. Direct tumor PO_2 measurement with physical probes has been used in clinical studies and is considered a reference standard. However, it is invasive and labor intensive. Another method is immunohistochemical (IHC) analysis of tumor biopsies based on hypoxia-associated endogenous proteins such as HIF-1α (22) and CA9 (23,24), or exogenous markers such as pimonidazole and EF5 that are preferentially trapped in hypoxic cells (25,26). The IHC approach is also invasive but can yield tumor hypoxia information with excellent spatial resolution for direct comparison with histology. A third approach involves nuclear imaging techniques such as single-photon emission computed tomography or positron emission tomography (PET), using hypoxia radiotracers, such as ^{18}F-FMISO, ^{18}F-EF5, ^{64}Cu-ATSM, and ^{124}I-IAZGP (9,27–30).

Reporter gene imaging is emerging as a valuable tool for studying tumor biology and deciphering genetic and biological processes in unperturbed microenvironment within experimental animals (31–36). In our previous efforts, applying this approach to the study of tumor hypoxia, Wen and colleagues (29) transduced Dunning rat prostate R3327-AT tumor cells with the vector 8HRE:tkeGFP, such that the fusion gene of HSV1-tk and enhanced green fluorescent protein (eGFP) was under the regulation of a hypoxia-inducible promoter containing eight tandem repeats of HRE (29). Similarly, Serganova and colleagues (37) used the same technique in C6 rat glioma cells. In hypoxic tumors, the reporter gene was expressed and the gene product TK phosphorylated the marker substrate ^{124}I-FIAU to generate microPET images. However, neither the transduced R3327-AT nor the C6 cells expressed eGFP at sufficient levels for unequivocal visualization in tumor sections, and hence, no such data were presented in reference 29 and 37. This was a major deficiency with these models because *in vivo* eGFP data, with its superb spatial resolution in optical imaging, is a valuable tool for studying microscopic tumor hypoxia distribution, as will be shown in this paper. Furthermore, both previous studies involved rodent tumor cells.

In this study, we developed a xenograft model using human tumor cells, to ensure the closest correspondence between our preclinical and clinical investigations of hypoxia imaging in colorectal tumor. Incorporating a 9HRE element provided by Dr. Dennis Deen (University of California, San Francisco, CA), we designed and constructed a new and improved

9*HRE:tkeGFP* vector, and transfected it into human colorectal adenocarcinoma HT29 cells. We then conducted a rigorous process of selection and enrichment, by repeated fluorescence-activated live cell sorting (FACS), to generate clones with the high level of hypoxia-induced TKeGFP expression. In *in vitro* studies, we verified the hypoxia-induced expression of the TKeGFP fusion protein by fluorescence microscopy and by quantifying TK-mediated trapping of ^{14}C-FIAU. In *in vivo* studies, PET and autoradiography were used to map the distributions of tumor hypoxia, based on hypoxia-induced TK expression and TK-mediated trapping of ^{124}I-FIAU. For direct comparison, similar distributions were obtained with the hypoxic cell radiotracer ^{18}F-FMISO in the same animals. In addition, fluorescence microscopy was used to visualize the eGFP distribution in tumor sections, in comparison of those of CA9, EF5, and pimonidazole.

Our results show that with this human xenograft reporter system, we can image hypoxia-induced molecular events and map their distribution *in vivo* with noninvasive PET imaging. This is based on hypoxia-induced increase in HIF-1α level, the downstream transcriptional activation of the *TKeGFP* fusion gene, and the TK-mediated phosphorylation and trapping of the marker substrate ^{124}I-FIAU *in vivo*. Thus, our model system provides a link between the molecular events of tumor hypoxia and noninvasive hypoxia imaging. It also allows us to examine the intratumoral distribution of various endogenous and exogenous hypoxia markers using dual-label phosphor plate imaging, IHC, and fluorescence microscopy. This human xenograft reporter model provides a valuable tool to study tumor hypoxia and in validating existing and future exogenous markers for tumor hypoxia.

Materials and Methods

Cell culture

Human colorectal carcinoma HT29 cells, obtained from American Type Culture Collection, were routinely cultured in Mc Coy's 5A medium, 10% fetal bovine serum, 2 mmol/L L-glutamine, 1.5 g/L sodium bicarbonate, 0.1 mmol/L nonessential amino acids, 1.0 mmol/L sodium pyruvate, and antibiotics.

Generation of hypoxia-inducible dual reporter expression vectors

The hypoxia-inducible, dual reporter expression plasmid p9HRE-TKeGFP contains the Herpes Simplex Virus type 1-thymidine kinase (*HSV1-tk*) and *eGFP* fusion gene under the regulation of a hypoxia-inducible promoter, and a constitutively expressed neomycin-resistance (*neo*^{r}) gene (Fig. 1*A*). The hypoxia-inducible promotor consists of an artificial nine tandem repeats of the HRE (9HRE) from the enhancer region of the human erythropoietin EPO gene, and was linked to the SV40 minimal promoter (SV40 min). The plasmid, pDsRed2-1 containing the constitutively expressed *neo*^{r} gene was purchased from BD Biosciences-Clontech. The *tkeGFP* cDNA fragment was excised from the retroviral vector dxHRE-tke/GFP-cmv Red2XPRT (37), placed under the control of the artificial 9HRE linked to the SV40 min, and cloned into pDsRed2-1, replacing the *DsRed2-1* gene. The resultant vector, designated as p9HRE-TKeGFP, was used to stably transfect human tumor HT29 cells. The DNA fragment of 9HRE is a generous gift from Dr. Dennis F. Deen (Brain Tumor Research Center of the Department of Neurological Surgery, University of California, San Francisco, CA; refs. 38, 39). Its DNA sequence is
GCTGCAGGAATTCGATGCACGCGTCCGGGTAGCTGGCGTACGTGCTGCAGCCGG
GTAGCTGGCGTACGTGCTGCAGCCGGGTAGCTGGCGTACGTGCTGCAGCTCGAG
ACTTGACGCGTCCGGGTAGCTGGCGTACGTGCTGCAGCCGGGTAGCTGGCGTAC
GTGCTGCAGCCGGGTAGCTGGCGTACGTGCTGCAGCTCGAGACTTGACGCGTCC
GGGTAGCTGGCGTACGTGCTGCAGCCGGGTAGCTGGCGTACGTGCTGCAGCCGG
GTAGCTGGCGTACGTGCTGCAG, with the italics marking the HRE tandem repeat.

Generation of stable cell lines containing the hypoxia-inducible dual reporter gene: transfection, clonal isolation, and enrichment

The HT29 cells were stably transfected with the dual reporter gene construct p9HRE-TKeGFP using calcium phosphate precipitation method (40–42). Colonies were selected and further enriched by repeated FACS gated for hypoxia-induced eGFP expression (Moflo cell sorter; Dako). In brief, the transfected cells were cultured in 400 μg/mL G418 for 3 to 4 wk. The drug-resistant cells were pooled and subjected to three cycles of FACS selection as follows. The cells were exposed to hypoxic condition (0.1% O_2) in an *In vivo* 2-400 hypoxic workstation for 24 h (Biotrace, Inc.), and then sorted by FACS based on the hypoxia-induced eGFP expression. The cells selected from the third sorting experiment were plated on 96-well plates (3 cells/mL; 200 μL per well). Individual clones (~60) were isolated, expanded, and transferred to mini vials and stored at −80°C.

Subsequently, we evaluated a number of the individual clones to identify the ones that have the maximum hypoxia inducibility. Cells were thawed, expanded, and transferred into duplicate sets of 24-well plates. One set of plated cells were exposed to 0.1% O_2 for 24 h, whereas the other remained in normoxic conditions. FACS was use to evaluated the eGFP signal in the hypoxic cells vis-à-vis that of the control. Based on these evaluations, two clones (designated as #C53 and #C5) were chosen and characterized in terms of growth kinetics, morphology, hypoxia-inducible TK activity, and xenograft formation in nude mice. Both clones showed similar characteristics, and clone #C53 was used for this study.

Induction of hypoxia in cell cultures

To induce hypoxia, monolayers of parental HT29 and #C53 were exposed to 0.1% O_2 in an *In vivo* 2-400 hypoxic workstation for different time intervals (29,40).

Radiotracer assay for TKeGFP expression *in vitro*

In vitro radiotracer accumulation studies with [^{14}C] 2′-Deoxy-2′-fluoro-β-D-arabinofuranosyl-5-iodouracil (^{14}C-FIAU) were performed to assess the hypoxia-induced TKeGFP expression (29). Briefly, #C53 cells (2×10^5 cells per well in 6-well plates) were exposed to 0.1% O_2 for different time intervals. After this treatment, the culture medium was replaced with medium containing ^{14}C-FIAU (Moravek Biochemicals; 0.025 μCi/mL; chemical purity, 97.7%) and incubated for 1 h at 37°C. The cells were then rinsed thrice with cold PBS and lysed with 1 mL of 0.3N NaOH/1% SDS. The lysates were neutralized (0.1 mL 3 N HCl) and assayed for protein level and ^{14}C-FIAU activity using a Wallac 1410 liquid scintillation counter. The ^{14}C-FIAU levels were normalized to the protein content of each sample. Under our experimental condition, no apparent quenching was observed.

Animal studies

Animal protocols were approved by the Institutional Animal Care and Use Committee at Memorial Sloan-Kettering Cancer Center (MSKCC). HT29 (parental) and #C53 tumors were formed by injecting 5×10^6 cells (in 50 μL) s.c. into the limbs of 6- to 8-wk-old female nude mice maintained under pathogen-free conditions (NCr athymic nu/nu; National Cancer Institute Frederick Cancer Research Institute; except that the data of Fig. 6*B* was obtained with male mice of the same strain as the females were not available from the vendor). The tumors grew to a diameter of ~6 and ~10 mm in 8 to 9 and 10 to 13 d, respectively.

In each experiment, 5 to 6 animals were used with three tumors per mouse, the parental on the shoulder, and the #C53 on the two hind limbs. All experiments were performed at least twice for reproducibility. The data from all the animals were compared, and representative results, consistent with that from the others, are presented here.

When the xenografts reached ~10 mm in diameter, serial microPET imaging was performed. A schematic of the *in vivo* imaging protocol using ^{18}F-FMISO and ^{124}I-FIAU tracers is given in Fig. 2*A*. Briefly, on day 1 of the experiment, nude mice each bearing 3 xenografts were injected i.v. with 1.5 mCi of ^{18}F-FMISO, and imaged with the microPET 2 h later. Immediately afterwards, the mice were injected with 630 μCi of ^{124}I-FIAU, and microPET imaging again performed 24 h later (day 2). Given the physical half-life of ^{18}F (1.83 h), the image on day 2 was due entirely to ^{124}I-FIAU (physical half-life of ^{124}I is 4.2 d). The thyroids of the animals were blocked by adding SSKI to their drinking water 1 d before ^{124}I-FIAU injection.

Immediately after the acquisition of the ^{124}I-FIAU images on day 2 (Fig. 2*A*), the tumor-bearing mice were injected i.v. with 2.2 mCi ^{18}F-FMISO and pimonidazole (80 mg/kg), so as to compare the intratumoral distributions of the tracers (^{124}I-FIAU and ^{18}F-FMISO) using autoradiographs (phosphor plate imaging). Two hours later, the mice were sacrificed. Thirty minutes before sacrifice, lectin-TRITC conjugate (for functional vessels; 100 mg/kg; Sigma-Aldrich), and 1 min before sacrifice, Hoechst 33342 (for perfusion; 25 mg/kg; Sigma-Aldrich) were injected i.v., respectively. After animal sacrifice, tumors were excised, snap frozen, and embedded in ornithine carbamyl transferase. Sections of 8-μm thickness were prepared for dual-tracer digital autoradiographs, IHC analysis, and fluorescence microscopy studies of the same and/or adjacent sections.

For *in vivo* studies involving reduced PO_2 environment, mice with #C53 xenografts (6–8 mm in diameter) were kept for 30 h in a custom-made, sealed-environmental chamber (VetEquip) that was infused with 10% oxygen and 90% nitrogen. In one experiment, EF5 (24 mg/kg) was coinjected i.v. with pimonidazole 2 h before sacrifice. Control mice with matched tumor volumes were maintained in room air.

Radioisotope production and radiochemical synthesis

^{18}F and ^{124}I were produced on the MSKCC cyclotron (TR19/9; EBCO Technologies, Inc.) using previously described techniques (29,35,43). ^{18}F-FMISO and ^{124}I-FIAU were synthesized as previously described (35,43). Unlabeled precursors were purchased from ABX GmbH.

Noninvasive PET imaging and dual-label phosphor plate imaging

For noninvasive imaging, the animals were anesthetized with isoflurane and imaged with the Focus 120 microPET, a small-animal PET scanner (Concorde Microsystems). PET images were acquired and reconstructed as previously described (30). In general, a minimum of ~10 million events were acquired in 5 to 40 min, depending on the radiotracer(s) injected, the administered activity, and the time postinjection (p.i.). The image data were corrected for nonuniformity of response of the microPET, dead time count losses, and physical decay. An empirically determined system calibration factor was used to convert voxel count rates (adjusted for the ^{124}I branching ratio) to activity concentrations, and the resulting data were then normalized to the administered activity to yield percent of the injected dose per gram of tissue (%ID/g or %ID/cc). Attenuation and scatter corrections were not applied because they are the same for the serial images and therefore unnecessary in image comparison.

To acquire the distributions of ^{124}I-FIAU and ^{18}F-FMISO with improved spatial resolution (of ~100 μm), dual exposure phosphor plate imaging was used (FUJI FILM). With this technique, the same specimen is used in two separate exposures. The first exposure was performed at the earliest possible time after tumor sectioning, for a duration of ~4 h. The resulting image was a composite of the signals from both ^{124}I-FIAU and ^{18}F-FMISO. The second exposure, initiated ~48 h later after the complete decay of ^{18}F, consists of the signal from longer-lived isotopic ^{124}I-FIAU only (half-life, 4.2 d). The duration of this second exposure was 48 h, to

allow sufficient signal accrual. To obtain the ^{18}F-FMISO image, we back decayed the second image (^{124}I-FIAU only) to obtain the contribution of ^{124}I-FIAU, and subtracted it from the first image (^{18}F-FMISO + ^{124}I-FIAU). Digital autoradiographs were processed using image analysis software (FUJI FILM Science Lab 2003). Image colocalization study was performed using the software package ImageJv1.38s (44,45).

IHC staining and fluorescence microscopy

Tumor sections were air dried for 30 min and fixed in ice-cold acetone for 20 min. Sections were incubated in SuperBlock (Pierce) for 30 min, and exposed to primary antibody diluted in blocking solution for 1 h at room temperature. Primary antibodies used were as follows: FITC-conjugated murine antipimonidazole monoclonal antibody (Chemicon) diluted 1:25; humanized anti-CA9 monoclonal antibody (cG250; a gift of Dr. Divgi, Memorial-Sloan Kettering Cancer Center, New York, NY; ref. 46), 25 μg/mL; and Cy3-conjugated anti-EF5 monoclonal antibodies (ELK3-51; a gift of Dr. Cameron J. Koch, University of Pennsylvania, Philadelphia, PA; ref. 47), 75 μg/mL. Sections were washed thrice with PBS and exposed to the appropriate secondary antibody for 1 h. CA9 was detected with an Alexa Fluor 568–conjugated goat anti-human antibody (Molecular Probes), 20 μg/mL. EF5 was detected with sheep anti-cyanine (5 μg/mL; USBiological) diluted in SuperBlock/mouse serum (1:1), and Alexa Fluor 568–conjugated anti-sheep antibody (20 μg/mL; Molecular Probes).

The sections were scanned on an image analysis system consisting of a Carl Zeiss Axiovert 200 mol/L fluorescence microscope using a computer-controlled motorized stage with a digital camera, and Metamorph software 7.0. All images were scanned at ×50 magnification. Composite images of sections were generated by the software from individual microscopic images. Sections were first imaged for eGFP, lectin-TRITC, and Hoechst, then stained for pimonidazole, EF5, and CA9, and imaged again with the appropriate markers visualized by green and red fluorescence, respectively. Finally the sections were stained with H&E according to standard protocol.

Results

In vitro characterization of human colorectal tumor HT29-9HRE-TKeGFP cells

As was described, the #C53 cells, containing the dual reporter HSV1-TKeGFP under the control of 9HRE, were selected in medium containing 400 μg/mL G418, and enriched by three cycles of FACS sorting of live cells gated for hypoxia-induced eGFP expression.

FACS analysis of hypoxia-induced eGFP expression, after incubating #C53 cells in air or at 0.1% O_2 for 24 hours, is shown in Fig. 1*B* and *C*. The scatter plots in Fig. 1*B*, and of the two histograms in Fig. 1*C*, clearly shows a significant increase in the expression of eGFP in hypoxic cells relative to that of the oxic cells. A comparison of the fluorescent microscopic images of hypoxic and aerated cells (Fig. 1*D*) showed that green fluorescence was observed only in the hypoxic cells, confirming the results of flow cytometric analysis. In Fig. 1*E*, the kinetics of hypoxia-induced expression of eGFP in #C53 cells are shown. Upon exposure to 0.1% O_2, the cellular eGFP expression assessed by FACS (Fig. 1*E*) increased with time, reaching half-maximum after ~8 to 12 hours, and a maximum (8–10 times that of control) after ~16 to 20 hours. No changes in eGFP expression were observed in the HT29 parental cells under hypoxic condition, or in #C53 cells under aerobic condition (data not shown).

Figure 1*F* shows the hypoxia-induced expression/function of TK to phosphorated FIAU in #C53 cells after exposure to 0.1% O_2 for various times, as assessed by ^{14}C-FIAU accumulation. Similar to the kinetics of hypoxia-induced eGFP expression (Fig. 1*E*), ^{14}C-FIAU uptake increased with time under hypoxia (Fig. 1*F*). ^{14}C-FIAU accumulation reached half maximum

after ~10 to 15 hours of hypoxia treatment, and the highest level (~20 times of control) after 20 to 25 hours.

Characterization of hypoxia-inducible HT29-9HRE-TKeGFP tumor model *in vivo*

To verify our *in vitro* findings, we performed experiments using transplanted tumors (~10 mm diameter) as was described in Fig. 2*A* (also see Materials and Methods). In Fig. 2*B*, the picture on the right illustrates the three tumors implanted in a nude mouse: parental (fore limb), and HT29-9HRE-TKeGFP (#C53) in both hind limbs. Serial microPET images are shown in the other two columns, with transverse images on the left and coronal images on the right. The top right panel (*coronal*) shows similar level of uptake of ^{18}F-FMISO in the HRE (*red arrows*) and the parental (*yellow arrow*) tumors, with heterogeneous distributions of activity within each of the xenografts. In contrast, the 24 h p.i. image of ^{124}I-FIAU uptake shows significant difference among the xenografts. There was no perceptible ^{124}I-FIAU accumulation in the parental HT29 tumor but significantly detectable and heterogeneous distribution of ^{124}I-FIAU in the #C53 xenografts (*bottom*). The patterns of the tracer uptake in the #C53 tumor are similar for ^{124}I-FIAU and ^{18}F-MISO (compare *top* and *bottom*), indicating that both are trapped in the same regions within the #C53 tumor. The middle panels are merged images of ^{18}F-FMISO and ^{124}I-FIAU. Similar serial microPET images were acquired from at least 10 animals, and yielded consistent results.

Phosphor plate imaging of ^{18}F-FMISO and ^{124}I-FIAU distribution

To compare the respective radioactivity distributions with improved spatial resolution, autoradiographs were acquired using phosphor plate imaging (see Materials and Methods; Fig. 2*A*). The middle panel of Fig. 3*A* were the second images, obtained at 48 hours p.i. of 2.2 mCi ^{18}F-FMISO. Given the 1.83 hours physical half-life of ^{18}F, these images were due entirely to ^{124}I-FIAU. We back-decayed these images to obtain the contribution of ^{124}I-FIAU, and subtracted it from the first image (obtained beginning ~6 hours p.i. of 2.2 mCi ^{18}F-FMISO and exposed for 4 h) to obtain the ^{18}F-FMISO image (Fig. 3*A*, *top*). Adjacent sections stained with H&E are shown in the bottom panels for comparison (Fig. 3*A*).

For the parental HT29 xenograft (Fig. 3*A*, *left*), the ^{124}I-FIAU image (*middle left*) is nearly blank, consistent with the expectation for this negative control. The first image shows a heterogeneous distribution of radioactivity due to ^{18}F-FMISO, indicative of tumor hypoxia. This first image is also consistent with the H&E image, in that there is negligible ^{18}F-FMISO accumulation in the lightly stained necrotic area. For the #C53 (HRE-TKeGFP) tumor, the ^{18}F-FMISO and ^{124}I-FIAU images are very similar and both indicate significant heterogeneity in tracer uptakes (comparing *top right* and *middle right*; Fig. 3*A*).

Digital autoradiograph images of ^{18}F-FMISO and ^{124}I-FIAU were processed using the image analysis software FUJI FILM Science Lab 2003. The ^{18}F-FMISO and ^{124}I-FIAU images were then coregistered and colocalization study performed using the software package Image J 1.38s (44,45). In Fig. 3*B*, the images of ^{18}F-FMISO (*red*), ^{124}I-FIAU (*green*), the overlay (yellow resulting from red plus green), and the correlation scatter plot are shown. The spatial distributions of ^{124}I-FIAU and ^{18}F-FMISO are very similar, as indicated by the Pearson's coefficient of 0.88.

Comparison of endogenous and exogenous hypoxic markers

Given the experimental protocol of Fig. 2*A*, we were able to study and compare the spatial relationship of various biomarkers, including Hoechst (perfusion), ^{124}I-FIAU, pimonidazole, eGFP, and CA9, in either the same or adjacent tumor sections. Figure 4 shows images obtained in one experiment: (*A*) H&E, (*B*) ^{124}I-FIAU autoradiogram, (*C*) eGFP, (*D*) Hoechst, (*E*) composite of eGFP and Hoechst, (*F*) magnified view of a region in *E*, (*G*) CA9, and (*H*)

pimonidazole. There was consistency in the observed distributions of the different biomarkers. In the necrotic zones, as identified in the H&E images, there was an absence of accumulation for all the tracers. The distributions of the endogenous markers eGFP and the exogenous reporter substrate ^{124}I-FIAU were identical as they should be because both stemmed from hypoxia-induced expression of the TKeGFP fusion protein. In addition, eGFP and ^{124}I-FIAU were most intense where there was low Hoechst staining, i.e., hypoxic regions with little perfusion. Similarly, the endogenous CA9 colocalizes with the exogenous pimonidazole but not with Hoechst. In general, there are good correlations in the spatial distributions of all four hypoxia markers, eGFP, ^{124}I-FIAU, CA9, and pimonidazole. The magnified view (*F*) of the fused image clearly shows that the hypoxia reporter eGFP (*green*) is in regions of low perfusion as indicated by low Hoechst staining.

The clear and unequivocal visualization of eGFP in #C53 tumor sections is a significant improvement relative to the previous R3327-AT and C6 models from this institution. The very high level of eGFP expression is likely the result of the 9HRE promoter and the repeated FACS sorting for selecting and isolating the #C53 cells. A careful examination of Fig. 4 shows low eGFP in necrotic regions (compare H&E section of *A* and the eGFP of *C*), high eGFP in viable but nonperfused regions (*F*), and concordance between eGFP pattern and those of the hypoxia-surrogates CA9 and pimonidazole. The white arrows and boxes in Fig. 4 (*C, E, G,* and *H*) highlight distinct features that illustrate the similarity in the distribution patterns of eGFP, CA9, and pimonidazole. These observations underline the usefulness of eGFP and the importance of the present tumor model for optical imaging of tumor hypoxia.

Figure 5 provides a more detailed examination and comparison of the different biomarkers in magnified views of a region from a HT29-9HRE-TKeGFP tumor (#C53). The top panels, from left to right, represent the following: (*A*) lectin-TRITC (functional blood vessels), (*B*) Hoechst (perfusion), (*C*) eGFP, (*D*) pimonidazole, and (*E*) CA9. The bottom row images are composites of two or three markers. The merged image of lectin-TRITC and Hoechst (Fig. 5*F*) shows functional blood vessels (*red*) surrounded by perfusion (*blue*), except for the vessel in the top right corner, which seems to be dysfunctional. The second from the left merged image (Fig. 5*G*) shows that eGFP (*green*) are located away from the blood vessels (*red*) and perfusion (*blue*), consistent with hypoxia-induced expression of the eGFP reporter gene. Also, in Fig. 5*H*, the exogenous hypoxic marker pimonidazole (*green*) is accumulated in regions of low perfusion, as is the endogenous hypoxic marker CA9 (*red*) in Fig. 5*I*. Lastly, the image in Fig. 5*J* shows colocalization of CA9 and pimonidazole (*yellow*, resulting from red plus green) in regions of low Hoechst.

As a further demonstration of the hypoxia-inducibility of the reporter system *in vivo*, we compared eGFP and pimonidazole in tumors of animals that breathed air vis-à-vis 10% O_2. In these experiments, we used ~6-mm diameter tumors that under normal conditions have low hypoxic fractions and low eGFP expression. Figure 6*A* (*a* and *b*) shows that there is little eGFP or pimonidazole in tumors of an air-breathing mouse, whereas there is high eGFP and pimonidazole signals in tumors of an animal breathing 10% O_2 (Fig. 6*A*, *c* and *d*). In another experiment, we compared the detailed spatial distributions of eGFP, pimonidazole, CA9, and EF5 in animals breathing air vis-à-vis 10% O_2. Whereas there was hardly any signal of these hypoxic markers in air-breathing animals (data not shown), there was significant accumulation of all 4 markers in the tumors of animals breathing 10% O_2 (Fig. 6*B*). These data clearly showed that the system is responsive to manipulation of tumor oxygenation.

Discussion

In this study, we established and evaluated a human xenograft model (#C53 or HT29-9HRE-TKeGFP) that links hypoxia-mediated molecular pathway to hypoxia imaging, specifically

optical imaging with IHC and noninvasive PET imaging. Because the expression of TKeGFP is a direct consequence of HIF-1α stabilization/HIF-1 transactivation, the first step of a major hypoxia-regulated molecular pathway, the level of the TKeGFP in the tumor is a surrogate of hypoxia-mediated HIF-1α stabilization/HIF-1 trans-activation and, thus, can serve as a reference for downstream events and other tumor hypoxia markers.

A very important element of the present study is the extremely high level of hypoxia-induced eGFP expression such that the intense green fluorescence signal can be easily visualized in freshly frozen tumor sections. This permitted, for the first time, eGFP optical imaging of hypoxia in tumor sections and provided a valuable tool for the study of endogenous and exogenous hypoxia markers *in vivo*. Optical imaging is easier to perform than nuclear imaging and, in this case, involves endogenous eGFP expression, thereby obviating the need of marker substrate (e.g., in bioluminescence imaging).

In this study, we showed the usefulness of this approach by comparing the distribution of eGFP with those of CA9, pimonidazole, EF5, and Hoechst in tumor sections. CA9, known to be regulated by the hypoxia-mediated signaling pathway in many cell types, has often been used as an endogenous surrogate for tumor hypoxia (23,24). In Figs. 4 and 5, it is shown that the distributions of eGFP and CA9 are well-correlated. Pimonidazole, FMISO, and EF5, members of the 2 nitroimidazole family of compounds, form adducts that become trapped within hypoxic cells and are commonly used in hypoxia studies (25). As shown in Figs. 4, 5, and 6, the spatial distributions of eGFP and pimonidazole are extremely similar under all experimental conditions. We believe that this provides evidence for the first time of the linkage between the initial hypoxia-induced molecular events, i.e., HIF-1α stabilization and HIF-1 transactivation, and the utility of 2 nitroimidazoles in marking tumor hypoxia *in vivo*.

To show the effect of tumor oxygenation manipulation on our model system, we compared the accumulation of eGFP, CA9, pimonidazole, and EF5 in animals breathing either 10% O_2 or air. Whereas there is little accumulation in air-breathing mice, there is high eGFP, CA9, EF5, and pimonidazole signals in mice breathing 10% O_2 (Fig. 6). In addition, the spatial distribution patterns of the four markers were similar.

Another important aspect of this tumor model is that the *HSV1-TK* gene is also expressed as a consequence of tumor hypoxia. This permits the use of noninvasive PET scanning with the marker substrate ^{124}I-FIAU to image hypoxia-induced gene expression and the associated spatial distribution of tumor hypoxia. Thus, the transactivation of the reporter gene by tumor hypoxia can be imaged in three-dimensional, generating a map of the molecular events associated with tumor hypoxia, i.e., hypoxia-induced HIF-1α stabilization leading to the reporter expression. This is shown by the PET images of Fig. 2. In addition, by comparing the respective PET images (Fig. 2), one can compare and spatially correlate the distributions of ^{124}I-FIAU (and the associated hypoxia-induced molecular events) and the exogenous hypoxia marker ^{18}F-FMISO, and validate the use of ^{18}F-FMISO in imaging tumor hypoxia.

To compare the distributions of ^{124}I-FIAU and ^{18}F-FMISO with better spatial resolution (relative to PET images), we used the dual-tracer autoradiographic technique. By sequentially exposing the same tumor section to the phosphor plate at different times p.i. of the two tracers, and exploiting the different physical half-lives of ^{124}I (4.2 h) and ^{18}F (1.83 h), we derived the respective distributions of ^{124}I-FIAU and ^{18}F-FMISO. As shown in Fig. 3*A*, the detailed spatial distributions of ^{124}I-FIAU and ^{18}F-FMISO seem identical in a #C53 tumor section. In contrast, they are totally disparate in the parental tumor because the HSV1-TK protein was absent, ^{124}I-FIAU cannot be phosphorylated and trapped inside the hypoxic cells. Statistical analysis showed that the spatial distributions of the two tracers are well-correlated in the #C53 tumor section (Fig. 3*B*).

As shown in Figs. 4 and 5, the multiparametric analysis of the different manifestations of tumor hypoxia generated a coherent picture. All the exogenous (pimonidazole and ^{18}F-FMISO) and endogenous markers (CA9) colocalize with the hypoxia-induced expression of eGFP, and with HSV1-TK as assessed by the trapping of the marker substrate ^{124}I-FIAU. In addition, they are located away from the perfused regions as marked by Hoechst staining.

In summary, we have developed and characterized a novel human xenograft model in which the hypoxia-induced molecular events can be visualized by either optical (fluorescent microscopy) or nuclear imaging (PET or autoradiography) techniques. Tumor hypoxia distributions determined by these methods have been compared with those measured by other surrogates (such as pimonidazole, EF5, ^{18}F-FMISO, and CA9), yielding excellent agreement. This system is responsive to manipulation of tumor oxygenation and provides a powerful tool for hypoxia research *in vitro* and *in vivo*, including those directed at therapeutic intervention targeting the hypoxia pathways.

Acknowledgments

Grant support: NIH grants CA56909, CA109772, and CA115675. This publication also acknowledges NCI grant P30-CA 08748, which provides partial support for the Research Animal Resource Center (RARC), Animal Imaging, Molecular Cytology and Flow Cytometry core facilities at MSKCC used in conducting this investigation.

We thank Dr. Dennis F. Deen for providing the 9HRE DNA fragment, Drs. Ronald Blasberg and Juri Gelovani for the plasmid containing tkeGFP fusion gene, and Maayan Korenblit for her assistance in the preparation of the manuscript.

References

1. Thomlinson R, Gray L. The histological structure of some human lung cancers and the possible implications for radiotherapy. Br J Cancer 1955;9:539–49. [PubMed: 13304213]
2. Brizel DM, Dodge RK, Clough RW, Dewhirst MW. Oxygenation of head and neck cancer: changes during radiotherapy and impact on treatment outcome. Radiother Oncol 1999;53:113–7. [PubMed: 10665787]
3. Hockel M, Schlenger K, Aral B, Mitze M, Schaffer U, Vaupel P. Association between tumor hypoxia and malignant progression in advanced cancer of the uterine cervix. Cancer Res 1996;56:4509–15. [PubMed: 8813149]
4. Nordsmark M, Overgaard J. A confirmatory prognostic study on oxygenation status and loco-regional control in advanced head and neck squamous cell carcinoma treated by radiation therapy. Radiother Oncol 2000;57:39–43. [PubMed: 11033187]
5. Brizel DM, Scully SP, Harrelson JM, et al. Tumor oxygenation predicts for the likelihood of distant metastases in human soft tissue sarcoma. Cancer Res 1996;56:941–3. [PubMed: 8640781]
6. Brizel DM, Rosner GL, Harrelson J, Prosnitz LR, Dewhirst MW. Pretreatment oxygenation profiles of human soft tissue sarcomas. Int J Radiat Oncol Biol Phys 1994;30:635–42. [PubMed: 7928495]
7. De Jaeger K, Merlo FM, Kavanagh MC, Fyles AW, Hedley D, Hill RP. Heterogeneity of tumor oxygenation: relationship to tumor necrosis, tumor size, and metastasis. Int J Radiat Oncol Biol Phys 1998;42:717–21. [PubMed: 9845083]
8. Fyles A, Milosevic M, Hedley D, et al. Tumor hypoxia has independent predictor impact only in patients with node-negative cervix cancer. J Clin Oncol 2002;20:680–7. [PubMed: 11821448]
9. Rasey JS, Koh WJ, Evans ML, et al. Quantifying regional hypoxia in human tumors with positron emission tomography of [18F]fluoromisonidazole: a pretherapy study of 37 patients. Int J Radiat Oncol Biol Phys 1996;36:417–28. [PubMed: 8892467]
10. Hockel M, Knoop C, Schlenger K, Vorndran B, Knapstein PG, Vaupel P. Intratumoral pO2 predicts survival in advanced cancer of the uterine cervix. Radiother Oncol 1993;26:45–50. [PubMed: 8438086]

11. Brizel DM, Sibley GS, Prosnitz LR, Scher RL, Dewhirst MW. Tumor hypoxia adversely affects the prognosis of carcinoma of the head and neck. Int J Radiat Oncol Biol Phys 1997;38:285–9. [PubMed: 9226314]
12. Graeber TG, Osmanian C, Jacks T, et al. Hypoxia-mediated selection of cells with diminished apoptotic potential in solid tumours. Nature 1996;379:88–91. [PubMed: 8538748]
13. Garcia S, Dales JP, Charafe-Jauffret E, et al. Poor prognosis in breast carcinomas correlates with increased expression of targetable CD146 and c-Met and with proteomic basal-like phenotype. Hum Pathol 2007;38:830–41. [PubMed: 17316758]
14. Koong AC, Denko NC, Hudson KM, et al. Candidate genes for the hypoxic tumor phenotype. Cancer Res 2000;60:883–7. [PubMed: 10706099]
15. Hockel M, Schlenger K, Mitze M, Schaffer U, Vaupel P. Hypoxia and radiation response in human tumors. Semin Radiat Oncol 1996;6:3–9. [PubMed: 10717157]
16. De Jaeger K, Kavanagh MC, Hill RP. Relationship of hypoxia to metastatic ability in rodent tumours. Br J Cancer 2001;84:1280–5. [PubMed: 11336482]
17. Reynolds TY, Rockwell S, Glazer PM. Genetic instability induced by the tumor microenvironment. Cancer Res 1996;56:5754–7. [PubMed: 8971187]
18. Rofstad EK, Rasmussen H, Galappathi K, Mathiesen B, Nilsen K, Graff BA. Hypoxia promotes lymph node metastasis in human melanoma xenografts by up-regulating the urokinase-type plasminogen activator receptor. Cancer Res 2002;62:1847–53. [PubMed: 11912164]
19. Semenza GL. Regulation of mammalian O2 homeostasis by hypoxia- inducible factor 1. Annu Rev Cell Dev Biol 1999;15:551–78. [PubMed: 10611972]
20. Semenza GL. Hypoxia-inducible factor 1 (HIF-1) pathway. Sci STKE 2007;2007:cm8. [PubMed: 17925579]Review
21. Chi JT, Wang Z, Nuyten DS, et al. Gene expression programs in response to hypoxia: cell type specificity and prognostic significance in human cancers. PLoS Med 2006;3:e47. [PubMed: 16417408]
22. Bussink J, Kaanders JH, van der Kogel AJ. Tumor hypoxia at the micro-regional level: clinical relevance and predictive value of exogenous and endogenous hypoxic cell markers. Radiother Oncol 2003;67:3–15. [PubMed: 12758235]
23. Wykoff CC, Beasley NJ, Watson PH, et al. Hypoxia-inducible expression of tumor-associated carbonic anhydrases. Cancer Res 2000;60:7075–83. [PubMed: 11156414]
24. Olive PL, Aquino-Parsons C, MacPhail SH, et al. Carbonic anhydrase 9 as an endogenous marker for hypoxic cells in cervical cancer. Cancer Res 2001;61:8924–9. [PubMed: 11751418]
25. Raleigh JA, Calkins-Adams DP, Rinker LH, et al. Hypoxia and vascular endothelial growth factor expression in human squamous cell carcinomas using pimonidazole as a hypoxia marker. Cancer Res 1998;58:3765–8. [PubMed: 9731480]
26. Koch CJ, Evans SM, Lord EM. Oxygen dependence of cellular uptake of EF5 [2-(2-nitro-1H-imidazol-1-yl)-N-(2,2,3,3,3-pentafluoropropyl)acetamide]: analysis of drug adducts by fluorescent antibodies vs bound radioactivity. Br J Cancer 1995;72:869–74. [PubMed: 7547233]
27. Dolbier WR Jr, Li AR, Koch CJ, Shiue CY, Kachur AV. [18F]-EF5, a marker for PET detection of hypoxia: synthesis of precursor and a new fluorination procedure. Appl Radiat Isot 2001;54:73–80. [PubMed: 11144255]
28. Chao KS, Bosch WR, Mutic S, et al. A novel approach to overcome hypoxic tumor resistance: Cu-ATSM-guided intensity-modulated radiation therapy. Int J Radiat Oncol Biol Phys 2001;49:1171–82. [PubMed: 11240261]
29. Wen B, Burgman P, Zanzonico P, et al. A preclinical model for non-invasive imaging of hypoxia-induced gene expression; comparison with an exogenous marker of tumor hypoxia. Eur J Nucl Med Mol Imag 2004;31:1530–8.
30. Zanzonico P, O'Donoghue J, Chapman JD, et al. i124-iodo-azomycin-galactoside (IAZG) imaging of tumor hypoxia in mice with serial microPET scanning. Eur J Nucl Med Mol Imag 2004;31:117–28.
31. Gambhir SS, Barrio JR, Phelps ME, et al. Imaging adenoviral-directed reporter gene expression in living animals with positron emission tomography. Proc Natl Acad Sci U S A 1999;96:2333–8. [PubMed: 10051642]

32. Glunde K, Shah T, Winnard PT Jr, et al. Hypoxia regulates choline kinase expression through hypoxia-inducible factor-1 α signaling in a human prostate cancer model. Cancer Res 2008;68:172–80. [PubMed: 18172309]
33. Nelson DW, Cao H, Zhu Y, et al. A noninvasive approach for assessing tumor hypoxia in xenografts: developing a urinary marker for hypoxia. Cancer Res 2005;65:6151–8. [PubMed: 16024616]
34. Ozawa T, Hu JL, Hu LJ, et al. Functionality of hypoxia-induced BAX expression in a human glioblastoma xenograft model. Cancer Gene Ther 2005;12:449–55. [PubMed: 15706354]
35. Tjuvajev JG, Avril N, Oku T, et al. Imaging herpes virus thymidine kinase gene transfer and expression by positron emission tomography. Cancer Res 1998;58:4333–41. [PubMed: 9766661]
36. Yu RM, Chen EX, Kong RY, Ng PK, Mok HO, Au DW. Hypoxia induces telomerase reverse transcriptase (TERT) gene expression in non-tumor fish tissues *in vivo*: the marine medaka (Oryzias melastigma) model. BMC Mol Biol 2006;7:27. [PubMed: 16961934]
37. Serganova I, Doubrovin M, Vider J, et al. Molecular imaging of spatial heterogeneity and temporal dynamics of hypoxia-induced HIF-1 signal transduction activity in tumors in living mice. Cancer Res 2004;64:6101–8. [PubMed: 15342393]
38. Chen JK, Hu LJ, Wang D, Lamborn KR, Deen DF. Cytosine deaminase/5-fluorocytosine exposure induces bystander and radiosensitization effects in hypoxic glioblastoma cells in vitro. Int J Radiat Oncol Biol Phys 2007;67:1538–47. [PubMed: 17394949]
39. Ruan H, Su H, Hu L, Lamborn KR, Kan YW, Deen DF. A hypoxia-regulated adeno-associated virus vector for cancer-specific gene therapy. Neoplasia 2001;3:255–63. [PubMed: 11494119]
40. He F, Li L, Kim D, et al. Adenovirus-mediated expression of a dominant negative Ku70 fragment radiosensitizes human tumor cells under aerobic and hypoxic conditions. Cancer Res 2007;67:634–42. [PubMed: 17234773]
41. Li GC, He F, Shao X, et al. Adenovirus-mediated heat-activated antisense Ku70 expression radiosensitizes tumor cells *in vitro* and *in vivo*. Cancer Res 2003;63:3268–74. [PubMed: 12810658]
42. Li GC, Li LG, Liu YK, Mak JY, Chen LL, Lee WM. Thermal response of rat fibroblasts stably transfected with the human 70-kDa heat shock protein-encoding gene. Proc Natl Acad Sci U S A 1991;88:1681–5. [PubMed: 1705702]
43. O'Donoghue JA, Zanzonico P, Pugachev A, et al. Assessment of regional tumor hypoxia using 18F-fluoromisonidazole and 64Cu(II)-diacetyl-bis(N4-methylthiosemicarbazone) positron emission tomography: Comparative study featuring microPET imaging, Po2 probe measurement, autoradiography, and fluorescent microscopy in the R3327-AT and FaDu rat tumor models. Int J Radiat Oncol Biol Phys 2005;61:1493–502. [PubMed: 15817355]
44. Abramoff MD, Magelhaes PJ, Ram SJ. Image processing with ImageJ. Biophotonics International 2004;11:36–42.
45. Rasband, WS. ImageJ, U. S. National Institutes of Health. Vol. 1. Bethesda; Maryland, USA: p. 1997-2007.
46. Steffens MG, Boerman OC, Oosterwijk-Wakka JC, et al. Targeting of renal cell carcinoma with iodine-131-labeled chimeric monoclonal antibody G250. J Clin Oncol 1997;15:1529–37. [PubMed: 9193349]
47. Lord EM, Harwell L, Koch CJ. Detection of hypoxic cells by monoclonal-antibody recognizing 2-nitroimidazole adducts. Cancer Res 1993;53:5721–6. [PubMed: 8242628]
48. Chaplin DJ. The effect of therapy on tumour vascular function. Int J Radiat Biol 1991;60:311–25. [PubMed: 1677988]
49. Shin KH, Diaz-Gonzalez JA, Russell J, et al. Detecting changes in tumor hypoxia with carbonic anhydrase IX and pimonidazole. Cancer Biol Ther 2007;6:70–5. [PubMed: 17172824]

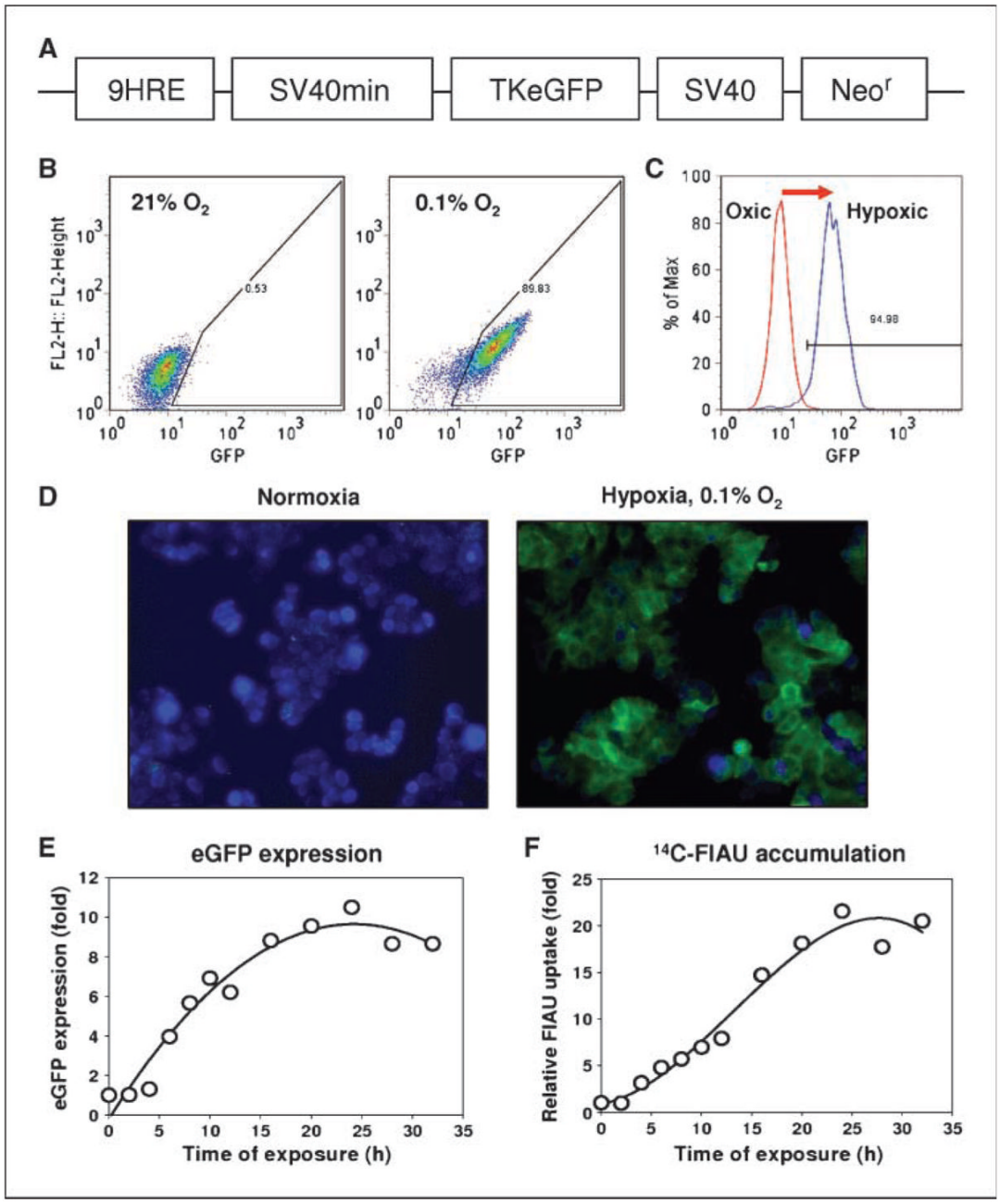

Figure 1.

Characterization of HT29-9HRE-TKeGFP dual reporter system *in vitro*. *A*, simplified diagram depicting the hypoxia-inducible 9HRE-TKeGFP construct. The expression vector p9HRE-SV40min-TKeGFP contains a HSV1-thymidine kinase and eGFP (*TKeGFP*) fusion gene under the regulation of a hypoxia-inducible promoter (nine tandem repeats of the hypoxia response element from the enhancer region of the human erythropoietin EPO gene linked to a SV40min promoter), and a SV40-driven neomycin-resistance (*Neo*^{r}) gene. *B*, HT29-9HRE cells (clone #C53) were exposed to 0.1% O_2 hypoxia or air for 24 h. The hypoxia-induced eGFP expression of individual cells was analyzed by flow cytometry and plotted as scattergrams. *C*, histogram representation of the data in *B*. It is clearly shown that 24-h incubation at 0.1% O_2 significantly increased the expression of eGFP of HT29-9HRE cells. *D*, fluorescent microscopy of

HT29-9HRE cells (clone #C53) incubated in either air (*left*) or 0.1% O_2 (*right*) for 24 h. Cells were fixed and stained with 4′-6′-diamidino-2-phenylindole (*blue*) and viewed using a Zeiss BX40 fluorescence microscope. eGFP expression is observed in a significant fraction of the hypoxic cells but is negligible in aerobic cells. *E*, kinetics of hypoxia-induced eGFP expression. After HT29-9HRE (#C53) cells were incubated in 0.1% O_2 for different time intervals, the eGFP expression were quantified by flow cytometric analysis and expressed as a ratio to that of aerated control. *F*, kinetics of hypoxia-induced TKeGFP expression/function as measured by ^{14}C-FIAU uptake. After HT29-9HRE (#C53) cells were incubated in 0.1% O_2 for different time intervals, the culture medium was replaced with medium containing ^{14}C-FIAU (0.025 μCi/mL) and incubated for 1 h at 37°C. The incorporated ^{14}C-FIAU activity was measured with a liquid scintillation counter and normalized to the protein content.

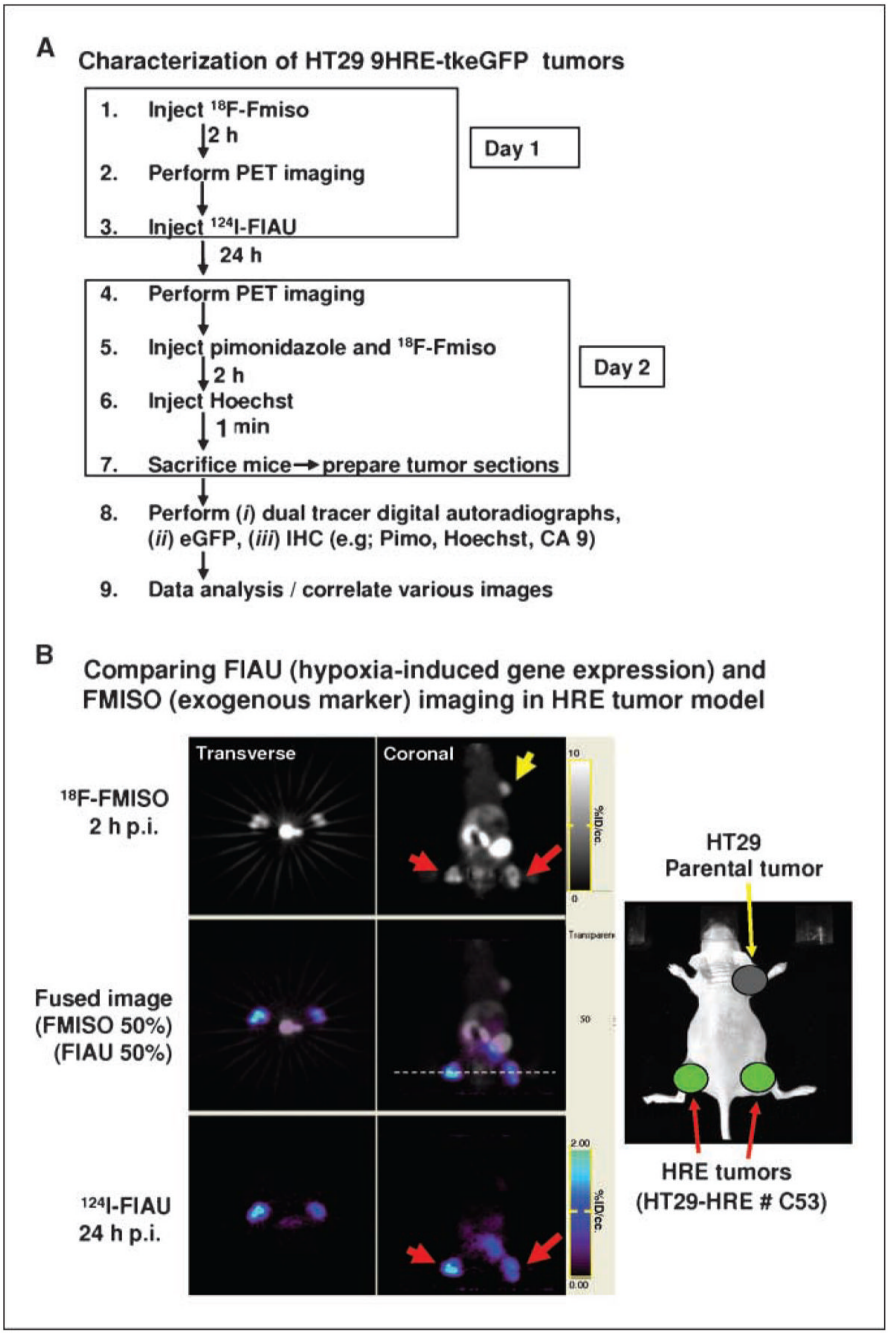

Figure 2.

Serial microPET imaging of HT29-9HRE-TKeGFP and parental tumors with ^{18}F-FMISO and ^{124}I-FIAU. *A*, schematics of the experimental protocol for sequential microPET imaging with ^{18}F-FMISO and ^{124}I-FIAU. *B*, comparing ^{124}I-FIAU (hypoxia-induced endogenous TK expression) and ^{18}F-FMISO (exogenous hypoxia marker) imaging in HT29-9HRE tumors. *Right*, the implantation of three tumors in a nude mouse: parental (fore limb) and HT29-9HRE in both hind limbs. Serial microPET images are shown in the two columns, with transverse images (0.8-mm thick sections; *left*) and coronal images (0.8-mm thick sections; *right*) shown. *Top right*, uptake of ^{18}F-FMISO in both the HRE tumors (*red arrows*) and the parental tumor (*yellow arrow*). In contrast, only the HRE tumors exhibited ^{124}I-FIAU uptake (*bottom right*).

The middle panels are merged images of ^{18}F-FMISO and ^{124}I-FIAU. The transverse images correspond to the position indicated by the white dashed line (*middle right*). The intensity scales were adjusted to individually optimize the display of ^{124}I-FIAU and ^{18}F-FMISO, respectively.

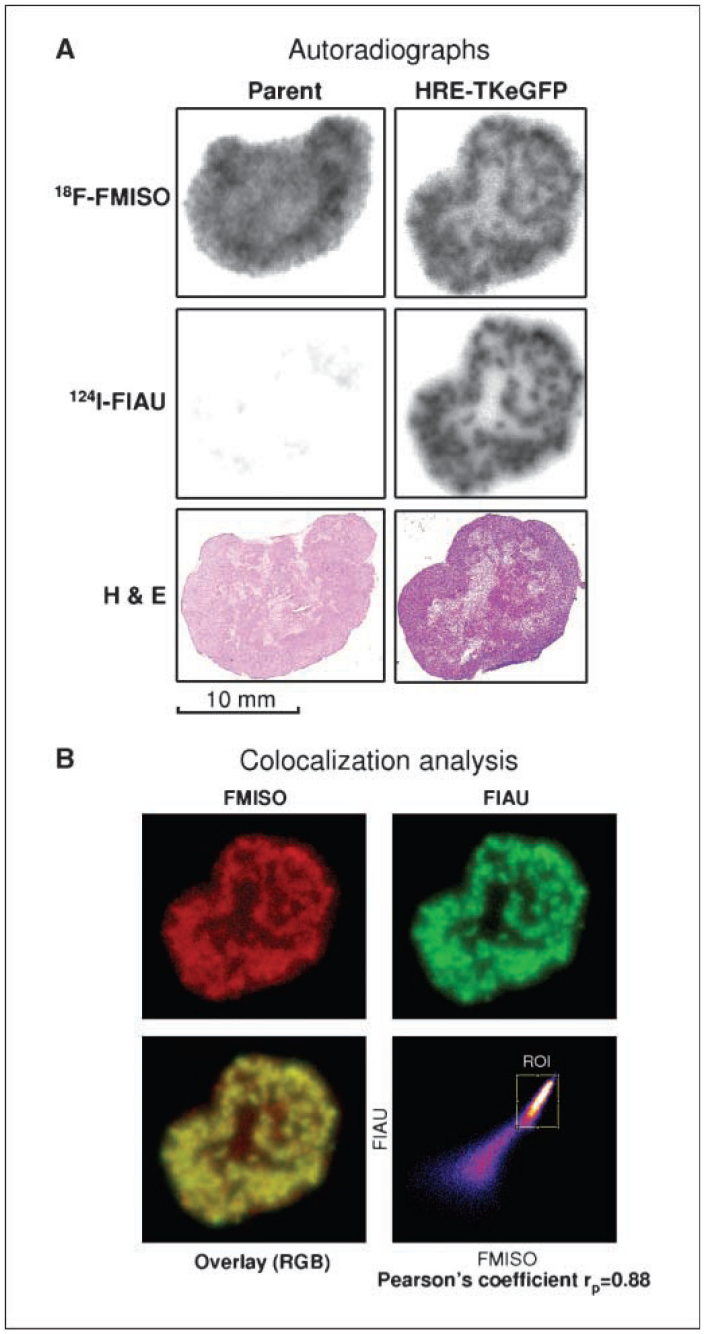

Figure 3.

Comparison of ^{124}I-FIAU and ^{18}F-FMISO autoradiographs. *A*, serial images were obtained in the same tumor sections with a phosphor plate imager (*top* and *middle*). Phosphor plate image of ^{18}F-FMISO radioactivity distributions was acquired first, followed by that of ^{124}I-FIAU (after complete decay of ^{18}F). We back decayed the ^{124}I-FIAU images (*middle*) and subtracted the contribution of ^{124}I-FIAU to the first image to obtain the ^{18}F-FMISO images (*top*). Adjacent sections stained with H&E are shown in the bottom for comparison. See text for details. *B*, the images of ^{18}F-FMISO (*red*; after subtracting the ^{124}I-FIAU contribution), ^{124}I-FIAU (*green*), the overlay (*yellow*), and the correlation scatter plot are shown (*ROI*, region of interest). The

spatial distributions of ^{18}F-FMISO and ^{124}I-FIAU are almost identical, as indicated by the Pearson's coefficient of 0.88.

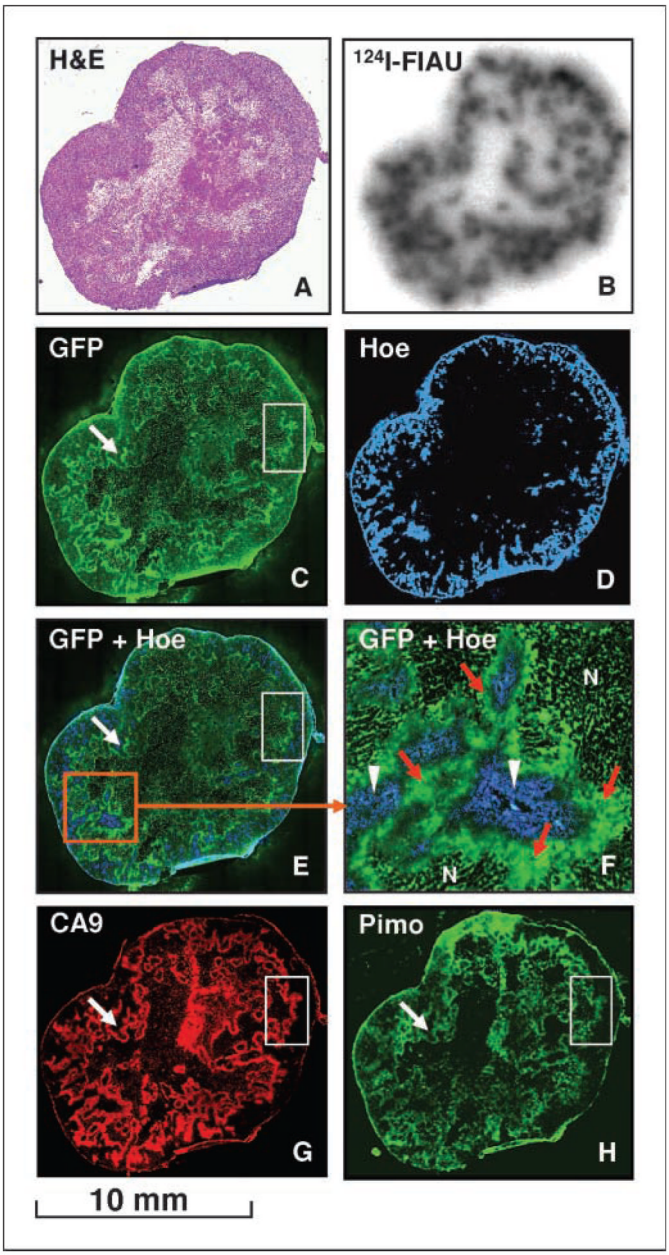

Figure 4.

Multiparametric comparison of tumor hypoxia markers in a #C53 xenograft. The distributions of the various hypoxia biomarkers in the same or adjacent tumor sections are shown as follows: (*A*) H&E; (*B*) ^{124}I-FIAU autroradiogram; (*C*) eGFP; (*D*) Hoechst (*Hoe; blue*); (*E*) composite of eGFP and Hoechst; (*F*) magnified view of a region in *E: N*, necrosis, hypoxia-induced eGFP expression (*green*; area also indicated by red arrows), and perfusion (*blue*; area also indicated by white arrowheads); (*G*) CA9 (*red*); and (*H*) pimonidazole (*Pimo; green*).

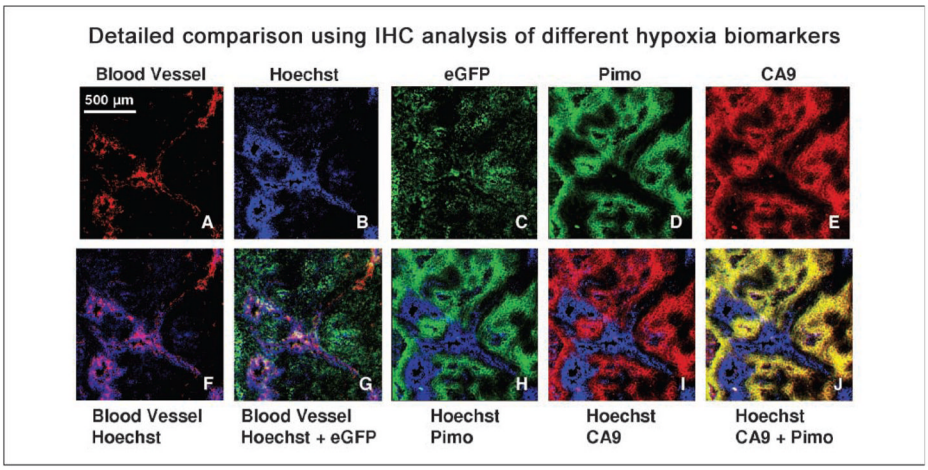

Figure 5.

Detailed comparison of the different biomarkers in a #C53 xenograft. *Top (from left to right)*, (*A*) lectin-TRITC (functional blood vessels), (*B*) Hoechst (perfusion), (*C*) eGFP, (*D*) pimonidazole, and (*E*) CA9. *Bottom*, merged images (*from left to right*), (*F*) lectin-TRITC (functional blood vessels in red) and Hoechst (perfusion in blue); (*G*) eGFP (*green*), blood vessels (*red*), and perfusion (*blue*); (*H*) pimonidazole (*green*) and Hoechst (*blue*); (*I*) CA9 (*red*) and Hoechst (*blue*); (*J*) CA9 (*red*) and pimonidazole (*green*) resulting in yellow regions where the two markers colocalize. All images were obtained from the same section and scanned at ×50 magnification. Section was first imaged for eGFP, lectin-TRITC, and Hoechst, then stained for pimonidazole and CA9. Control experiment showed that TRITC and eGFP did not interfere with Alexa 568 and FITC signals, respectively (data not shown). Pimonidazole at higher doses (300 mg/kg) have been reported to interfere with blood flow in KHT tumors growing in mice (48). However, at the dose of 80 mg/kg, perfusion images of HT29 tumors did not indicate a loss of blood flow (49).

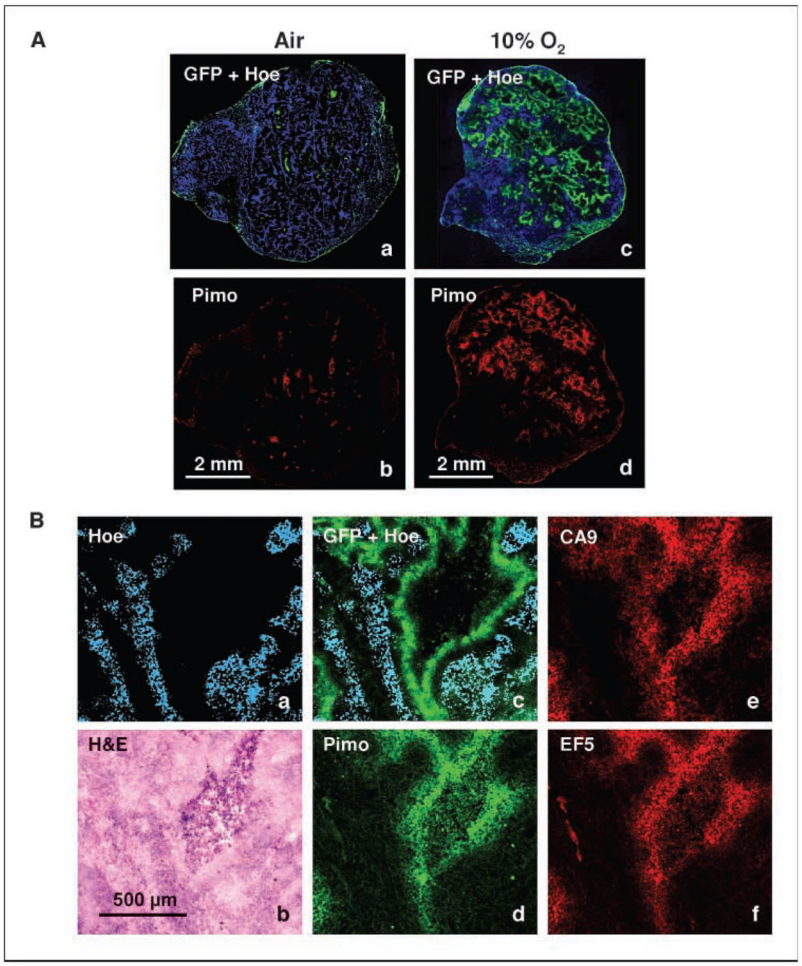

Figure 6.

The effect of breathing 10% O_2 on tumor hypoxia. *A*, HT29-9HRE (#C53) tumor-bearing mice were placed in a custom-made 10% O_2 chamber for 30 h, or sham-treated, and then sacrificed. The animals were injected i.v. with pimonidazole (2 h before sacrifice) and Hoechst (1 min before sacrifice). Frozen tumor sections were made, and eGFP expression, pimonidazole, and Hoechst images were acquired. Comparison of tumor sections from animals that breathed air or 10% O_2 are shown. *Left and right*, tumor sections from air-breathing (*a* and *b*) and 10% O_2-breathing (*c* and *d*) mice, respectively. *B*, similar to *A* above, except that EF5 was coinjected with pimonidazole, and CA9 distribution was also obtained. In air-breathing animals, there was hardly any accumulation of any of the markers (data not shown). *a*, Hoechst; *b*, H&E; *c*, Hoechst + eGFP; *d*, pimonidazole; *e*, CA9; *f*, EF5 (all images were from the same section except that EF5 was from an adjacent section). Note the similarity in the spatial distributions of the four hypoxic markers, away from the Hoechst staining areas and surrounding a necrotic region.